

1 **Supplement File**

2 **Machine learning significantly improves the simulation of hourly-to-**
3 **yearly scale cloud nuclei concentration and radiative forcing in**
4 **polluted atmosphere**

5 Jingye Ren^{1,2}, Songjian Zou³, Honghao Xu³, Guiquan Liu³, Zhe Wang³, Anran Zhang³,
6 Chuanfeng Zhao⁴, Min Hu⁵, Dongjie Shang⁵, Lizi Tang⁵, Ru-Jin Huang¹, Yele Sun⁶,
7 Fang Zhang^{3*}

8 ¹State Key Laboratory of Loess Science, Institute of Earth Environment, Chinese Academy of
9 Sciences, Xi'an, 710061, China

10 ²Xi'an Institute for Innovative Earth Environment Research, Xi'an, 710061, China

11 ³Shenzhen Key Laboratory of Organic Pollution Prevention and Control, School of Eco-
12 Environment, Harbin Institute of Technology Shenzhen, Shenzhen, 518055, China

13 ⁴Department of Atmospheric and Oceanic Sciences, School of Physics, Peking University, Beijing,
14 100871, China

15 ⁵State Key Joint Laboratory of Environmental Simulation and Pollution Control, College of
16 Environmental Sciences and Engineering, Peking University, Beijing, 100871, China

17 ⁶State Key Laboratory of Atmospheric Boundary Layer Physics and Atmospheric Chemistry,
18 Institute of Atmospheric Physics, Chinese Academy of Sciences, Beijing, 100029, China

19

20 Corresponding author: Fang Zhang, zhangfang2021@hit.edu.cn

21

22

23

24

25

26 **Data and Methods**

27 **S1. WRF-Chem model**

28 In this study, WRF-Chem v 4.1.5 is used to simulate CCN concentration for
29 training the machine learning model. The physical parameterizations employed in this
30 study include Morrison 2-moment scheme (Morrison et al., 2009), RRTMG short-
31 wave and long-wave radiation scheme (Iacono et al., 2008), Grell 3-D cumulus scheme
32 (Grell et al., 2002), Yonsei University boundary layer scheme and Noah land surface
33 model (Hong et al., 2006). The Carbon Bond Mechanism Z photochemical mechanism
34 and 4-bin sectional Model for Simulating Aerosol Interactions and Chemistry
35 (MOSAIC) aerosol model with aqueous chemistry are chosen in this study (Zaveri et
36 al., 1999, 2008). The initial meteorological variables are provided from the National
37 Center for Environmental Prediction's Final Operational Global (NCEP/FNL) datasets.
38 The horizontal resolution of the reanalysis data was $0.25^{\circ} \times 0.25^{\circ}$, and the temporal
39 resolution was 6 h. The initial and boundary chemical conditions are from the
40 Community Atmosphere Model with Chemistry model (Buchholz et al., 2019). The
41 anthropogenic emissions are from Multi resolution Emission Inventory for China with
42 a horizontal resolution of $0.25^{\circ} \times 0.25^{\circ}$ and a temporal resolution of monthly data (Zheng
43 et al., 2018), corresponding to the years 2014-2018. The biological and biomass
44 emissions are taken from the Model of Emissions of Gases and Aerosols from Nature
45 and the Fire Inventory from NCAR, respectively.

46 S2. Evaluation of the aerosol indirect effects

47 Atmospheric particles acting as cloud condensation nuclei could alter the cloud-
48 rain interactions and further have impact on the climate change. The methods for
49 evaluating the cloud and radiative properties caused by the deviations of CCN
50 concentrations output from WRF-Chem simulation and random forest technique was
51 refereed from Wang et al. 2019 and Wang et al. 2008.

52 As for the first indirect effect, the cloud optical thickness (τ) and single scatter
53 albedo coefficient (ω_0) are the crucial estimators and can be calculated as:

$$54 \quad \tau \approx \frac{3}{2} W r_e^{-1} \quad (1)$$

$$55 \quad 1 - \omega_0 = 1.7 k_w r_e \quad (2)$$

56 where W means the liquid water path, k_w is the complex part of the refractive index of
57 water, r_e is the effective radius of cloud droplets and can be expressed by:

$$58 \quad r_e = \beta \left(\frac{3LWC}{4\pi\rho_w N_c} \right)^{1/3} \quad (3)$$

59 where LWC is the liquid water content in cloud, β is the scaling factor. Here, we mainly
60 focused on the response of cloud droplet effective radius to the change of cloud droplet
61 number concentration N_c , so β is assumed to be constant (Quaas et al., 2004). Cloud
62 number concentration can be calculated based on the N_{CCN-SS} parameterizations in
63 many climate models (Fan et al., 2012). Note that the power relationship between the
64 r_e and N_c referred from the previous observations is only an approximate relationship
65 (Garrett et al., 2004).

66 For evaluating second aerosol indirect forcing, it is critical to estimate the relevant
 67 variables associated with the cloud-rain process. The parameterizations of the cloud-to-
 68 rain conversion process can be expressed by conversion threshold function (TA):

$$69 \quad TA = \frac{\left[\int_{r_c}^{\infty} r^6 n(r) dr \right]}{\left[\int_0^{\infty} r^6 n(r) dr \right]} \frac{\left[\int_{r_c}^{\infty} r^3 n(r) dr \right]}{\left[\int_0^{\infty} r^3 n(r) dr \right]} \quad (4)$$

70 where r is the cloud droplet radius, $n(r)$ is the size distribution of the cloud droplet (here
 71 refereed from Wang et al. 2019 to evaluate). According to the Liu et al. (2004), the
 72 critical radius of the auto-conversion process r_c can be expressed by

$$73 \quad r_c \approx 4.09 \times 10^{-4} \beta_{con}^{1/6} \frac{N_C^{1/6}}{LWC^{1/3}} \quad (5)$$

74 where β_{con} is a fixed parameter of $1.15 \times 10^{23} \text{ s}^{-1}$ (Liu et al., 2004). Here, the focus is
 75 mainly on the effect of the ΔN_{CCN} between WRF-Chem and RF model on the aerosol
 76 indirect effects in our research.

77 We also evaluate the perturbation of cloud radiative forcing due to the uncertainty
 78 in CCN concentration estimated from machine learning (RFRM) and numerical model
 79 (WRF-Chem). Here under the assumption of the fixed liquid water volume, an
 80 approximate analytical expression for estimating the cloud radiative of the change in
 81 N_{CCN} as follows (Charlson et al, 1992; Wang et al., 2008):

$$82 \quad \Delta F_C \approx -\frac{F_T}{4} A_{mst} T_r^2 \Delta R_C \approx -2.2 \times \Delta \ln N_{CCN} \quad (6)$$

$$83 \quad \Delta R_C = \frac{1}{3} [R_C (1 - R_C)] \times \Delta \ln N_d \approx 0.075 \times \Delta \ln N_d \quad (7)$$

$$84 \quad \Delta \ln N_d \approx 0.5 \times \Delta \ln N_{CCN} \quad (8)$$

85 where ΔF_c is the uncertainty in cloud radiative forcing, F_T is the solar constant, A_{mst} is
 86 the cloud fractional coverage, T_r is the fractional transmission of shortwave radiation
 87 above the cloud layer, ΔR_c is the uncertainty in cloud albedo, N_d is the cloud droplet

88 number concentration, N_{CCN} is the cloud condensation nuclei number concentration. In
89 equation (6), A_{mst} and T_r were set as 0.3 and 0.76, respectively (Charlson et al, 1987;
90 Schwartz et al., 1996), which represented an average fraction of nonoverlapped marine
91 stratus and stratocumulus. Here the uncertainty in ΔR_c in equation (7) for the typical
92 range of cloud albedo was calculated according to the Wang et al. 2008. The uncertainty
93 N_d associated with change in N_{CCN} was referred from Sotiropoulou et al. (2006) with a
94 value of 0.5 in equation (8).

95 **References**

- 96 Buchholz, R. R., Emmons, L. K., Tilmes, S., & The CESM2 Development Team.:
97 CESM2.1/CAM-chem Instantaneous Output for Boundary Conditions.
98 UCAR/NCAR - Atmospheric Chemistry Observations and Modeling Laboratory.
99 e.g. Lat: -10 to 10, Lon: 100 to 150, September 2015 - February 2016, 2019.
- 100 Charlson, R. et al.: Climate Forcing by Anthropogenic Aerosols, *Science*, 255, 423–430,
101 <https://doi.org/10.1126/science.255.5043.423>, 1992.
- 102 Charlson, R. et al.: Oceanic phytoplankton, atmospheric sulphur, cloud albedo and
103 climate, *Nature*, 326(6114), 655–661, <https://doi.org/10.1038/326655a0>, 1987.
- 104 Fan, J., Leung, L. R., Li, Z. et al.: Aerosol impacts on clouds and precipitation in eastern
105 China: Results from bin and bulk microphysics, *Journal of Geophysical Research*,
106 117, D00K36, <https://doi.org/10.1029/2011JD016537>, 2012.
- 107 Garrett, T. J., Zhao, C., Dong, X., Mace, G.G., Hobbs, P.V.: Effects of varying aerosol
108 regimes on low-level arctic stratus, *Geophysical Research Letters*, 31,
109 <https://doi.org/10.1029/2004GL019928>, 2004.
- 110 Grell, G. A., Dezsó, D.: A generalized approach to parameterizing convection
111 combining ensemble and data assimilation techniques, *Geophysical Research*
112 *Letters*, 29, 1693, <https://doi.org/10.1029/2002GL015311>, 2002.
- 113 Hong, S. Y., Noh, Y., Dudhia, J.: A new vertical diffusion package with an explicit
114 treatment of entrainment processes, *Mon. Weather Rev*, 134(9), 2318,
115 <https://doi.org/10.1175/MWR3199.1>, 2006.

116 Iacono, M. J., Delamere, J. S., Mlawer, E. J. et al.: Radiative forcing by long-lived
117 greenhouse gases: calculations with the AER radiative transfer models, *Journal of*
118 *Geophysical Research: Atmospheres*, 113 (D13), [https://doi.org/](https://doi.org/10.1029/2008JD009944)
119 [10.1029/2008JD009944](https://doi.org/10.1029/2008JD009944), 2008.

120 Liu, Y., Daum, P. H., & McGraw, R.: An analytical expression for predicting the critical
121 radius in the autoconversion parameterization, *Geophysical Research Letters*, 31,
122 L06121, <https://doi.org/10.1029/2003GL019117>, 2004.

123 Morrison, H., Thompson, G., Tatarskii, V.: Impact of cloud microphysics on the
124 development of trailing stratiform precipitation in a simulated squall line:
125 Comparison of one-and two-moment schemes, *Monthly Weather Review*, 137(3),
126 991–1007, <https://doi.org/10.1175/2008MWR2556.1>, 2009.

127 Quaas, J., Boucher, O., & Breon, F. M.: Aerosol indirect effects in POLDER satellite
128 data and the Laboratoire de Meteorologie Dynamique Zoom (LMDZ) general
129 circulation model, *Journal of Geophysical Research*, 109, D08205,
130 <https://doi.org/10.1029/2003JD004317>, 2004.

131 Schwartz, S. E. and Slingo, A.: Enhanced shortwave cloud radiative forcing due to
132 anthropogenic aerosols., in: *Clouds, Chemistry, and Climate.*, edited by: Crutzen,
133 P., and Ramanathan, V., Springer, Heidelberg. 191–236, 1996.

134 Sotiropoulou, R. E. P., Medina, J., and Nenes, A.: Ccn predictions: Is theory sufficient
135 for assessments of the indirect effect?, *Geophysical Research Letters*, 33, L05816,
136 <https://doi.org/10.1029/2005GL025148>, 2006.

137 Wang, Y., Niu, S., Lv, J. et al.: A new method for distinguishing unactivated particles in
138 cloud condensation nuclei measurements: implications for aerosol indirect effect
139 evaluation, *Geophysical Research Letters*, 46, 14,185–14,194,
140 <https://doi.org/10.1029/2019GL085379>, 2019.

141 Wang, J., Lee, Y.-N., Daum, P. H., Jayne, J., and Alexander, M. L.: Effects of aerosol
142 organics on cloud condensation nucleus (CCN) concentration and first indirect
143 aerosol effect, *Atmos. Chem. Phys.*, 8, 6325–6339, [https://doi.org/10.5194/acp-8-](https://doi.org/10.5194/acp-8-6325-2008)
144 [6325-2008](https://doi.org/10.5194/acp-8-6325-2008), 2008.

145 Zaveri, R. A., Peters, L. K.: A new lumped structure photochemical mechanism for
146 large-scale applications, *Journal of Geophysical Research: Atmospheres*, 104,
147 30387–30415, <https://doi.org/10.1029/1999JD900876>, 1999.

148 Zaveri, R. A., Easter, R. C., Fast, J. D. et al.: Model for simulating aerosol interactions
149 and chemistry (MOSAIC), *Journal of Geophysical Research: Atmospheres*,
150 113(D13), <https://doi.org/10.1029/2007JD008782>, 2008.

151 Zheng, B., Tong, D., Li, M. et al.: Trends in China's anthropogenic emissions since
152 2010 as the consequence of clean air actions, *Atmos. Chem. Phys.*, 18, 14095–
153 14111, <https://doi.org/10.5194/acp-18-14095-2018>, 2018.

154 **Table S1.** Summary of the datasets used in this study from multiple sources

Data category	Content (Abbreviation)	Unit	Spatial resolution	Temporal resolution	Data source
N_{CCN}	CCN concentration (N_{CCN}) at $S=0.20\%$ and $S=0.40\%$	cm^{-3}	10 km	Hourly	WRF-Chem model
Chemical compositions	Organic matter (OM) Sulfate (SO_4^{2-}) Nitrate (NO_3^-) Ammonium (NH_4^+)	$\mu\text{g m}^{-3}$ $\mu\text{g m}^{-3}$ $\mu\text{g m}^{-3}$ $\mu\text{g m}^{-3}$	10 km - - -	Daily - - -	TAP (http://tapdata.org.cn/?page_id=59&item=pm25)
Meteorological data	2m temperature (TEM) Relative humidity (RH) Boundary layer (BL) Surface pressure (SP) Surface net solar radiation (SNSR)	K % M hPa W m^{-2}	$0.25^\circ \times 0.25^\circ$ - - - -	Hourly - - - -	ERA-5 (https://cds.climate.copernicus.eu/cdsapp#!/dataset/reanalysis-era5-single-levels?tab=form)
Gas pollutants	PM _{2.5} NO ₂ SO ₂ CO O ₃	$\mu\text{g m}^{-3}$ - - - -	- - - - -	Hourly - - - -	CEMC (https://quotsoft.net/air/)

155

Figures

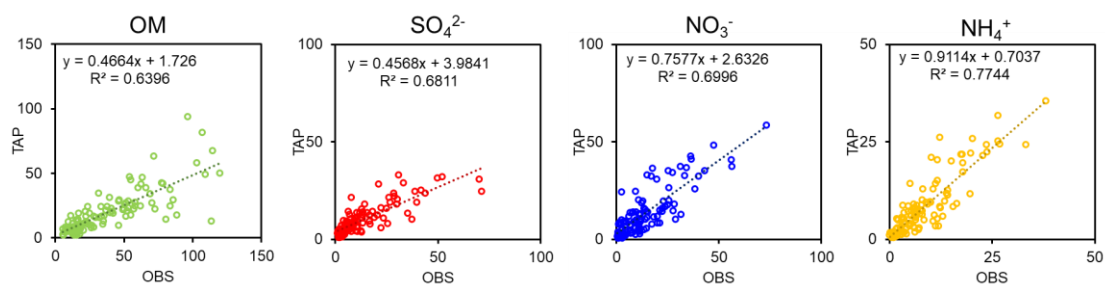


Figure S1. Comparison of the mass concentration of organic, sulfate, nitrate, ammonium between the TAP dataset and observed values at BJ site.

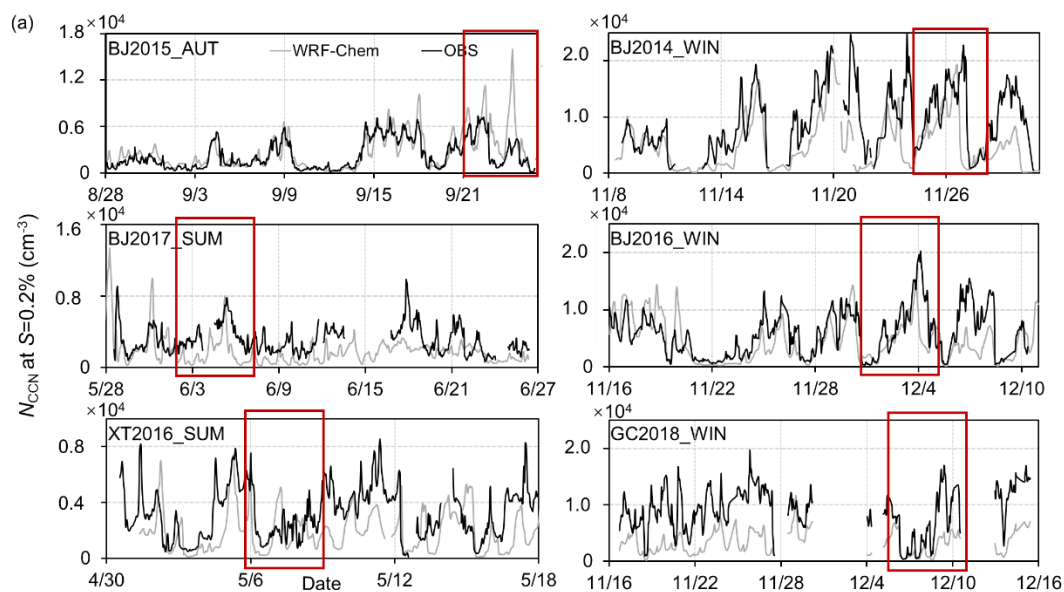


Figure S2. Time series of the WRF-Chem simulated and observed N_{CCN} at $S=0.2\%$ for the six campaigns, red box indicates the validation dataset.

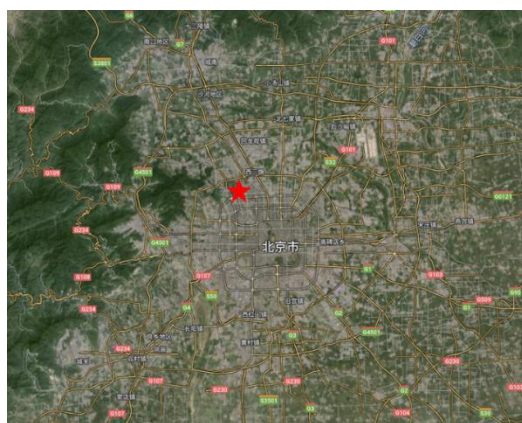


Figure S3. Map location of the sampling site (red star represents the Peking University). (Imagery © 2025 NASA, Map data © 2025 Google, <https://maps.google.com/>, last access: 8 September 2024).

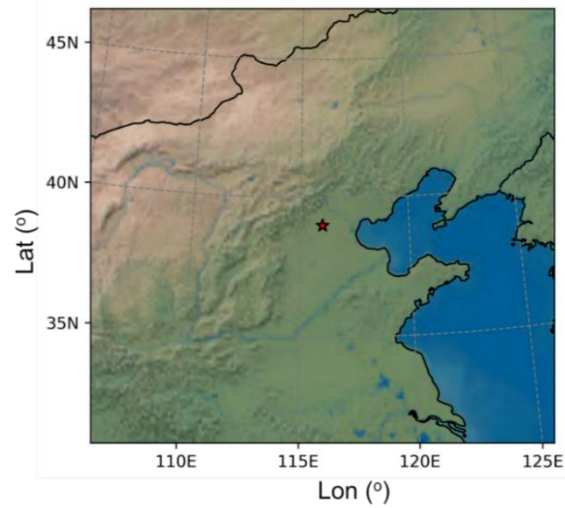


Figure S4. WRF-Chem model simulation domain diagram drawn by using the Cartopy library. Red star represents the center point of the simulation domain.

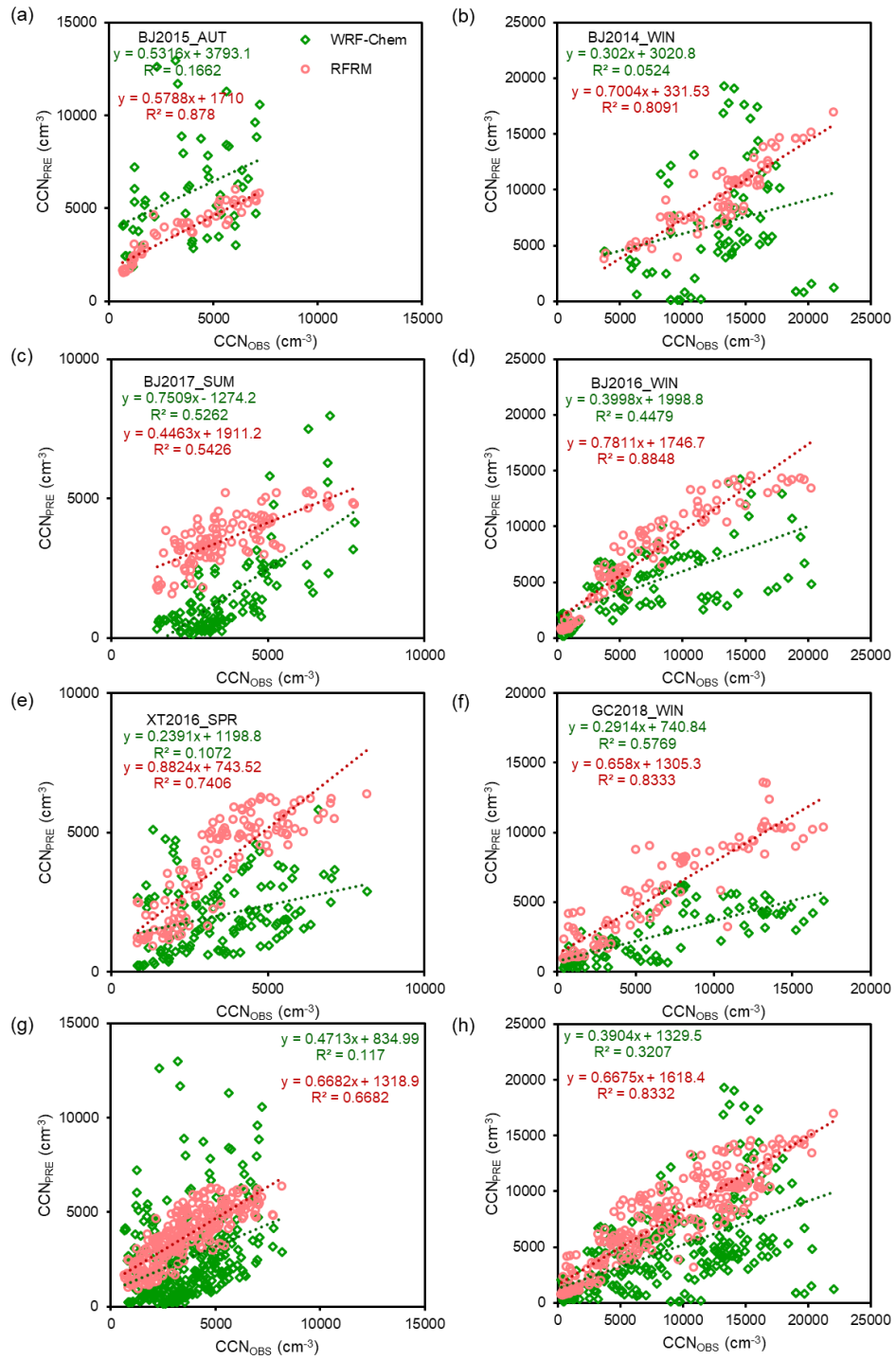


Figure S5. Scatter plots of the observed N_{CCN} with the RFRM-predicted and WRF-Chem-simulated for each campaign at $S=0.2\%$.

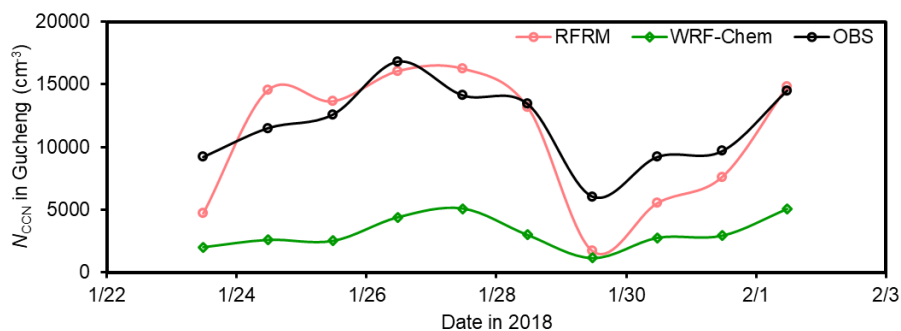


Figure S6. Time series of the RFRM-predicted, WRF-Chem simulated and observed N_{CCN} at $S=0.2\%$ at Gucheng.

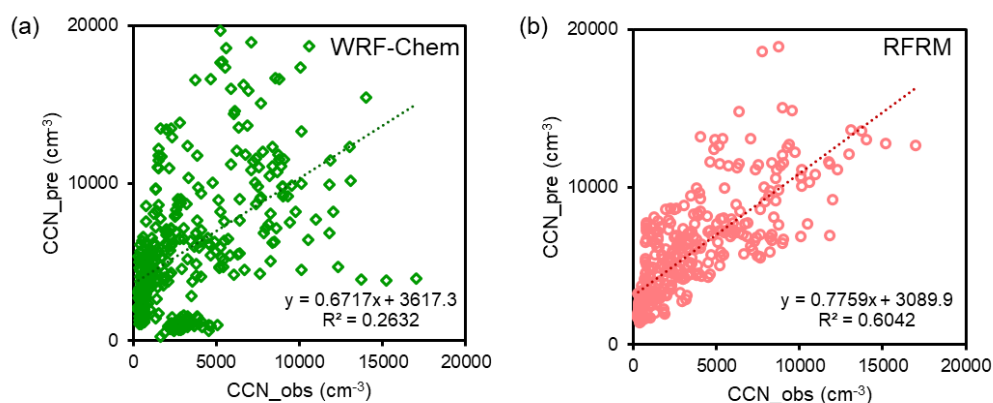


Figure S7. Scatter plots of the observed N_{CCN} at $S=0.4\%$ with the WRF-Chem simulated and RFRM model predicted, respectively. Here the training, testing, and validation datasets are independent of the period corresponding to the supersaturation of 0.2%.

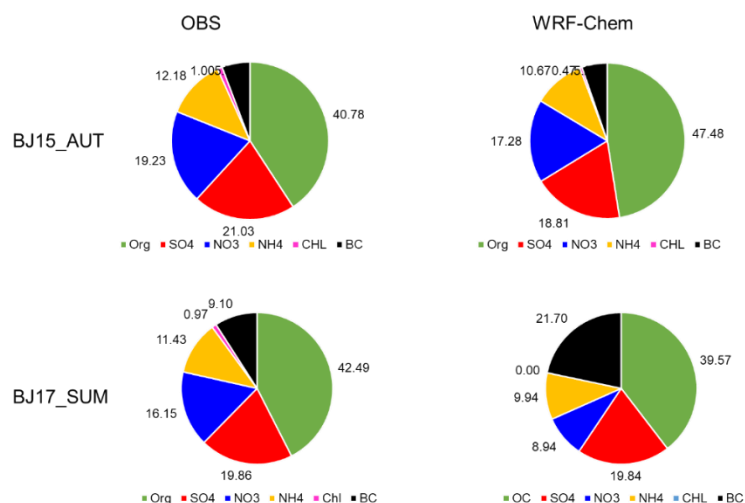


Figure S8. Pie charts of the mass fraction of the chemical composition between the observation and simulation from WRF-Chem, taken the BJ15_AUT and BJ17_SUM as the examples.

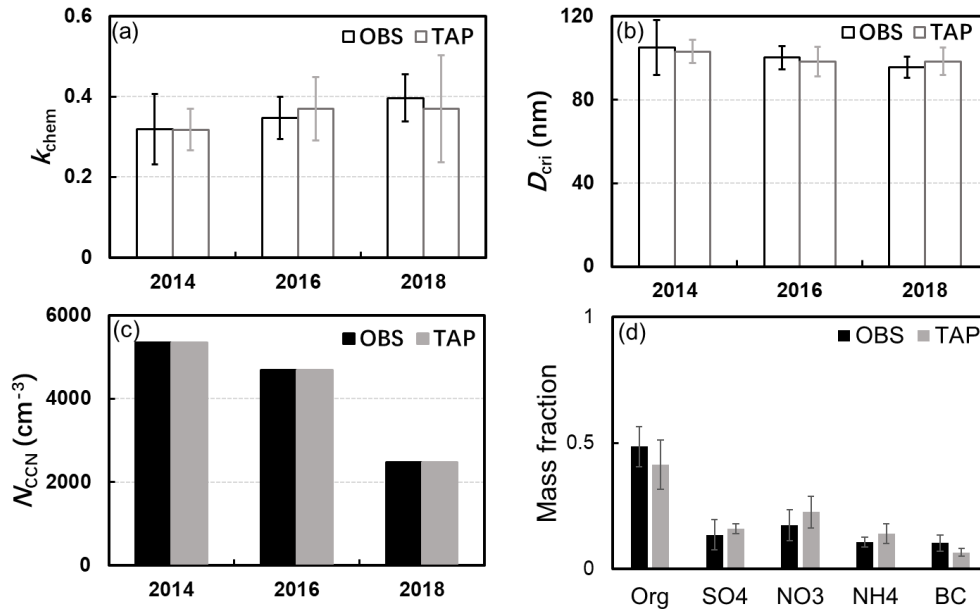


Figure S9. Average annual value of the k_{chem} calculated from chemical composition (a), the critical diameter at $S=0.2\%$ (b), N_{CCN} at $S=0.2\%$ (c), the mass fraction (d) between the observed and TAP dataset in the winter of 2014, 2016, 2018.

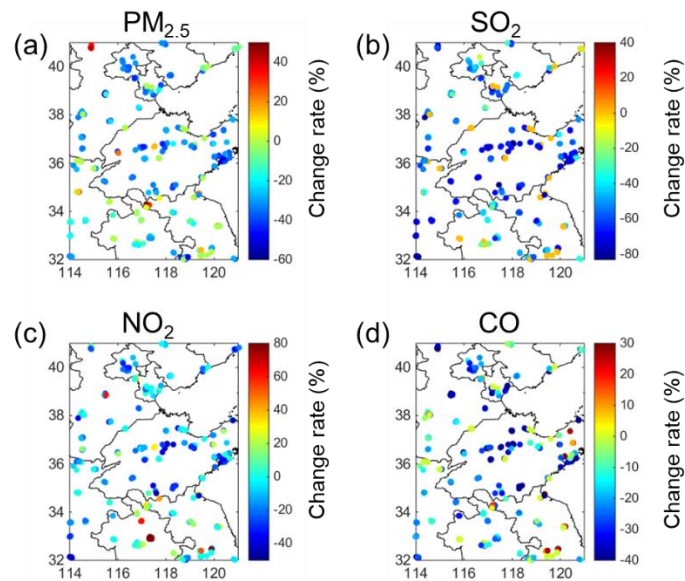


Figure S10. Spatial pattern of the change rates of the $PM_{2.5}$, SO_2 , NO_2 and CO from 2014 to 2018 in NCP.

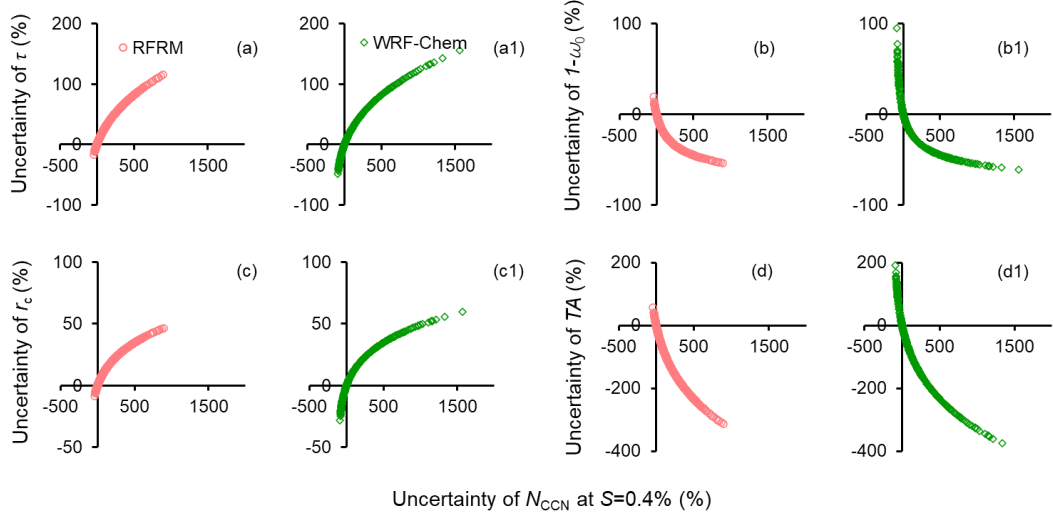


Figure S11. Sensitivity of the cloud properties on the CCN concentration at $S=0.4\%$, uncertainty of the CCN number concentration on cloud optical thickness (τ) between the observed with the RFRM model (a) and with the WRF-Chem model (a1), on absorption coefficient ($1-\omega_0$) and effective radius (r_c) (b and b1), on critical radius (r_c) (c and c1), the cloud-to-rain conversion threshold function (TA) (d and d1).

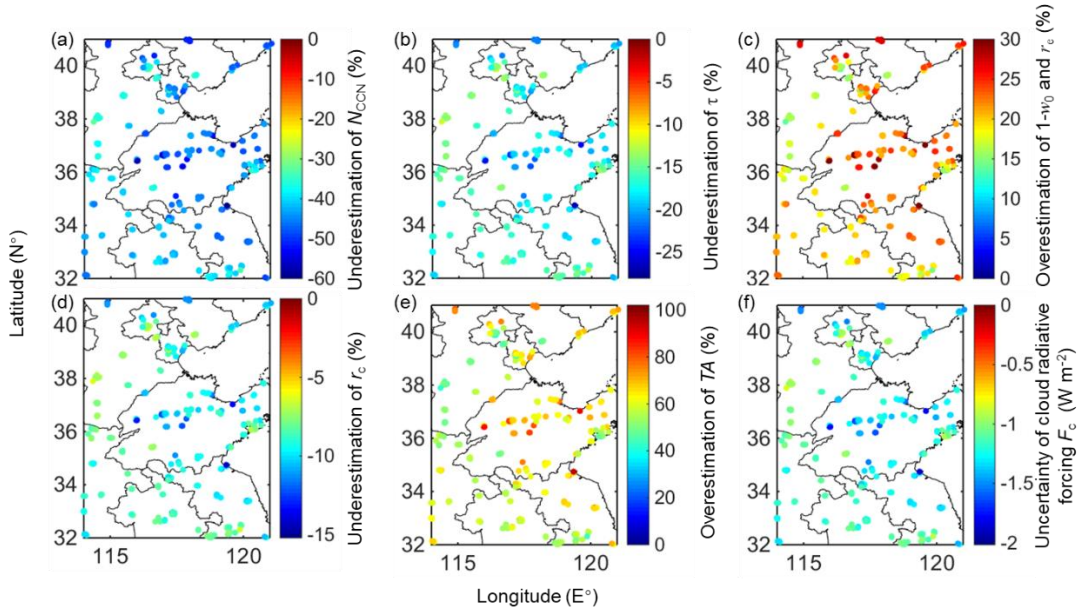


Figure S12. Spatial pattern of the differences of CCN number concentration between the RFRM model and WRF-Chem (a), effects of the discrepancy from CCN number concentration on cloud optical thickness (τ) (b), on absorption coefficient ($1-\omega_0$) and effective radius (r_c) (c), on critical radius (r_c) (d), the cloud-to-rain conversion threshold function (TA) (e), cloud radiative forcing (F_c) (f).